Correlation of fluorescence evolution for quantitative analysis of labels and sensors

Agnès Pellissier-Tanon, Beatrice Adelizzi, Thomas Le Saux, Annie Lemarchand, Ludovic Jullien

Correlation of fluorescence evolution for quantitative analysis of labels and sensors

Agnès Pellissier-Tanon,[1†] Beatrice Adelizzi,[1†] Ludovic Jullien,[1]
Thomas Le Saux,[1*] Annie Lemarchand[2*]

[1]PASTEUR, Département de chimie, École normale supérieure,
PSL University, Sorbonne Université, CNRS, 24 rue Lhomond, 75005 Paris, France

[2]Sorbonne Université, Centre National de la Recherche Scientifique (CNRS),
Laboratoire de Physique Théorique de la Matière Condensée (LPTMC),
4 place Jussieu, case courrier 121, 75252 Paris Cedex 05, France

[†]These authors contributed equally to this work.

E-mail: agnes.pellissier-tanon@ens.psl.eu, beatrice.adelizzi@ens.psl.eu, ludovic.jullien@ens.psl.eu, thomas.lesaux@ens.psl.eu, annie.lemarchand@sorbonne-universite.fr.

[*]To whom correspondence should be addressed:
Annie Lemarchand (+331 4427 4455), Thomas Le Saux (+331 4432 2406)

Abstract Titration without separation, e.g. quantification of a target species in living cells, is a challenge of analytical chemistry. We perform the selective detection of a target using the kinetics involved in a photochemical process and develop a correlation method that we illustrate by the titration of a fluorescent photoswitcher and the target of a photoswitching sensor. Correlating an input time series and a well-chosen weighting function associated with a variable characteristic time yields a spectrum of characteristic times. The upper integration limit of the correlation output can be chosen to match the argument of an extremum of the spectrum with a characteristic time of the input time series in order to quantify the target. A similar procedure is followed to optimize the signal-to-noise ratio. Selectivity and signal-to-noise ratio associated with 15 weighting functions are theoretically predicted. The results are applied to the titration of the reversibly photoswitchable fluorescent protein Dronpa-2 and the titration of calcium using a reversibly photoswitchable fluorescent sensor. The performance of the correlation method is favorably compared to the one of other dynamic contrast protocols.

Keywords titration, correlation, characteristic times, signal-to-noise ratio, reversibly photoswitchable fluorescent protein, calcium sensor

1 Introduction

Quantifying a targeted species in a mixture is a major task of analytical chemistry. It may rely on a step of separation, which facilitates quantification by providing purified fractions. However, this invasive approach cannot be applied to complex mixtures such as living cells which have to remain native. In this case, the design of highly selective and separation-free protocols is crucial. Spectroscopic signatures are often harnessed. However, due to spectral crowding, the intrinsic spectroscopic signature of the targeted species is often hidden in the signal of the mixture and hardly singularized. The target can be more easily discriminated after derivatization with a fluorescent label that stands out from the mixture under illumination at well chosen wavelengths. Then, the concentration of the target can be retrieved from the detection of fluorescence. In addition to the spectroscopic signature, the kinetics involved in the photochemical process brings specific information and improves the selective detection of the label related to the targeted species.

The kinetics-based discrimination strategy has found various developments in fluorescence analysis and imaging.[1] Hence, the minimal absorption–fluorescence emission photocycle has been used to discriminate spectrally overlapping fluorophores harnessing the lifetime of their excited states in Fluorescence Lifetime Imaging Microscopy (FLIM).[1, 2] More recently, the reversibly photoswitchable fluorophores (RSFs) have been exploited to introduce several protocols of dynamic contrast imaging. Transient state imaging microscopy (TRAST) monitors the dynamics of the long-lived, photo-induced transient dark states of RSFs.[3] Synchronously amplified fluorescence imaging recovery (SAFIRe) exploits long-lived RSF dark states, which are depopulated under modulated illumination at a secondary wavelength higher than fluorescence emission.[4] Out-of-Phase Imaging after Optical Modulation (OPIOM) exploits a periodically modulated illumination at one or two wavelengths and adds the phase lag of the RSF modulated fluorescence signal to the frequency-dependent modulation amplitude exploited by SAFIRe as a further control parameter leading to the discrimination fo four fluorophores.[5, 6, 7, 8] Bleaching-Assisted Multichannel Microscopy (BAMM) exploits the specific kinetic signature of RSF photobleaching.[9] Four fluorophores are discriminated using the time-integrated fluorescence under tailored illuminations.[10] Eventually, four kinetic regimes of the rich photocycles of RSFs are harnessed to discriminate 20 RSFs over 22 using LIGHTNING.[11]

Most dynamic contrast protocols focus on tailoring illumination to target a given photoswitchable fluorophore. Optical Lock-In Detection (OLID) introduces a post-acquisition processing and correlates the fluorescence signal of a reversibly photoswitcher under periodic illumination with a reference signal or function.[12, 13, 14] The Deep Level Transient Spectroscopy (DLTS) used to study electrically active defects in semiconductors is also based on the correlation between an input time series and a weighting function.[15, 16, 17, 18, 19]

We introduce a separation-free titration method inspired from OLID and DLTS. Light intensity or any control parameter is tuned to promote the variation of an observable of interest. We choose to observe the relaxation of fluorescence intensity of photoswitchable fluorophores for given initial conditions. In order to titrate a species associated with a given photoswitching characteristic time, we introduce the correlation of the input fluorescence time series with a weighting function associated with the same characteristic time. The accuracy of the titration depends on the sensitivity of the correlation output to the noise affecting the input time series. Correlation outputs can be computed for an interval of characteristic times of the weighting function leading to a spectrum of characteristic times. In the case of a mixture of photoswitchable fluorophores, the better the result of the titration of a given target, the smaller the correlation outputs of the interfering fluorophores determined at the characteristic time of the target. Consequently, the accuracy of the titration depends on the bandwidth of the spectrum of characteristic times. We perform a theoretical analysis and discuss the optimization of signal-to-noise ratio and selectivity depending on the weighting function. Using different scalings of the correlation output, we apply the correlation method to either the direct quantification of the concentration of a targeted reversibly photoswitchable fluorescent protein (RSFP) or the titration of calcium in interaction with a one-color ratiometric reversibly photoswitchable fluorescent sensor.[20, 21]

The manuscript is organized as follows. Section 2 provides Material and Methods. In section 3, we study the signal-to-noise ratio and the bandwidth of the spectrum of characteristic times for different weighting functions and a theoretical input time series. Two different versions of the correlation output are considered. The theoretical predictions are experimentally validated in section 4. The correlation method is applied to the titration of the reversibly photoswitchable fluorescent protein Dronpa-2 using a correlation output proportional to the concentration of the fluorophore.[5, 6, 11, 22] Using a different scaling, we harness the reaction of calcium with a reversibly photoswitchable fluorescent sensor and employ the correlation method to titrate calcium.[20, 21] We conclude in section 5.

2 Materials and Methods

Materials Solvents and chemicals are obtained from Aldrich. Buffered calcium solutions ($[Ca^{2+}] = 0$ and 38.8 μM) for GCaMP6s-Q experiments are purchased from Thermo Fisher Scientific. Both aqueous solutions contain 30 mM 3-(N-morpholino)propanesulfonic acid (MOPS), 100 mM KCl, pH = 7.2. The solution buffered at $[Ca^{2+}] = 0$ additionally contains 10 mM EGTA (Ethylene glycol-bis(2-aminoethylether)-N,N,N',N'-tetraacetic acid); the solution buffered at $[Ca^{2+}]$ = 38.8 μM contains 10 mM CaEGTA. All home-made solutions are prepared with freshly de-ionized water from a MilliQ system.

Protein production and purification Plasmids expressing Dronpa-2 and GCaMP6s-Q carrying an N-terminal hexahistidine tag are transformed in an *E. coli* LB21 strain.[23] Cells are grown in Lysogeny broth (LB) and expression is induced at the optical density at 600 nm OD_{600} = 0.6 by addition of isopropyl β-D-1-thiogalactopyranoside (IPTG) to obtain a final concentration of 1 mM. Cells are harvested by centrifugation (4000 *g* for 20 min at 4 °C) after 16 h expression at 20 °C and then frozen. The cell pellet is resuspended in lysis buffer (PBS buffer: 50 mM phosphate buffer, NaCl 150 mM, and $MgCl_2$ 5 mM, DNAase 5 mg mL^{-1}, PMSF 1 mM, pH = 7.4) and sonicated (5 min at 20 % of amplitude, 3 s on, 1 s off). Insoluble material is removed by centrifugation and the soluble proteins are adsorbed onto Ni-NTA agarose resin suspended in phosphate-buffered saline (PBS: Na_3PO_4 50 mM, NaCl 150 mM, pH 7.4) via overnight incubation at 4 °C under gentle agitation. The protein loaded Ni-NTA beads are inserted in a column and washed (20·vol, 50 mM PBS + 20 mM imidazole, 5 mL 50 mM PBS + 40 mM imidazole). Bound proteins are then eluted with 5 mL 50 mM PBS + 500 mM imidazole. GCaMP6s-Q is then dialyzed in dialysis cassettes with 2 L TBS buffer (0.1 M TBS buffer (tris(hydroxymethyl)aminomethane), 300 mM NaCl, pH = 7.4) and stored at -20 °C. Dronpa-2 is dialyzed in dialysis cassettes with PBS buffer, pH = 7.4) and stored at -20 °C.

Preparation of the solutions For Dronpa-2, a stock solution is prepared in PBS with [Dronpa-2] = 7 μM and stored at -20 °C for a maximum of three months. The operating Dronpa-2 solutions are prepared by diluting the stock solution with PBS (pH = 7.4) to the desired concentration.

For GCaMP6s-Q, two stock solutions ([GCaMP6s-Q] = 8 μM) are prepared by diluting GCaMP6s-Q (stored in TBS) with each of the solutions of Thermo Fisher kit (see above). The calcium concentrations of the stock solutions ([Ca^{2+}] = 0 and 39 μM) are corrected to take into account the variation of the dissociation constant of CaEGTA with respect to the ionic strength using GCaMP6s-Q stored solutions. The stock solutions are stored at -20 °C for a maximum of one month. The operating solutions at asymptotic calcium concentrations ([GCaMP6s-Q] = 1 μM and [Ca^{2+}] = 0 or 38.8 μM) are prepared by diluting the stock solutions with the adequate Thermo Fisher buffer. The operating solutions at intermediate [Ca^{2+}] are obtained by cross-dilution between the [GCaMP6s-Q] = 1 μM solutions at [Ca^{2+}] = 0 and 38.8 μM, as recommended by the manufacturer. For each measurement, all the operating solutions are freshly prepared and left at rest at room temperature for approximately 1 h before use.

Fluorimeter setup Fluorescence measurements used for kinetic analysis are performed in a fluorescence cuvette (1.5 mm optical path, 60 μL) at 20 °C on a LPD220 spectrofluorometer (PTI, Monmouth Junction, NJ) equipped with a TLC50 cuvette holder (Quantum Northwest, Liberty Lake, WA) thermoregulated with a Peltier temperature controller. Light intensities

are controlled by varying the current that powers two light-emitting diodes (LED). The first LED (LXZ1-PB01 from Philips Lumileds, San Jose, CA) is filtered at 480 ± 20 nm (HQ 480-40 from Chroma Technology Corp, Rockingham, VT), and the second LED (LHUV-0405, Philips Lumileds) is filtered at 405 ± 20 nm (F405-40; Semrock, Rodchester, NY). The LEDs are supplied by a DC4100 LED driver (Thorlabs, Newton, NJ). The two light sources are collimated with ACL2520U condenser lenses (Thorlabs) and then the beams are combined using a dichroic filter (T425LPXR, Chroma Technology Corp) in order to deliver homogeneous illumination over the whole sample. The fluorescence evolution is recorded at 515 nm.

In a first step, light intensities are calibrated using Dronpa-2 for which the photoisomerization cross-section $\sigma_{480} = 196$ m^2.mol^{-1} under illumination at 480 nm is known.[5, 6] A monoexponential function is fitted to the fluorescence evolution of Dronpa-2 under illumination at 480 nm. For a sufficiently large light intensity I_{480}, the resulting relaxation time τ_m is used to deduce I_{480} according to[6, 11]

$$I_{480} = \frac{1}{\sigma_{480}\tau_m} \tag{1}$$

In a second step, the samples are first submitted to a constant illumination of intensity I_{480} = 0.0045 ± 0.0003 Ein m^{-2} s^{-1} at 480 nm during 1 s, then a constant illumination of intensity I_{405} = 0.005 Ein m^{-2} s^{-1} at 405 nm during 1 s, and finally a constant illumination of intensity I_{480} = 0.0045 ± 0.0003 Ein m^{-2} s^{-1} at 480 nm during 1 s. The first illumination at 480 nm is used to erase the history of the sample and discarded.

Epifluorescence setup Microscopy experiments are performed in a home-built epifluorescence microscopy setup. Measurements are performed in a coverslip glass chamber (80 μm thickness) containing homogenous protein solutions.

The samples are illuminated using LXZ1-PB01 LED (Philips Lumileds) filtered at 480 nm ± 20 nm (F480-40; Semrock, Rodchester, NY) and a LHUV-0405 (Philips Lumileds) LED filtered at 405 ± 20 nm (F405-40; Semrock, rochester, NY). Each LED is supplied by a LED driver (LEDD1B, Thorlabs, Newton, NJ) and controlled by a waveform generator (33612 A, Keysight Technologies). A lens (ACL2520U; Thorlabs, Newton, NJ, f = 20 mm) is placed just after each diode to collimate the light sources. The two light beams are then combined using a dichroic mirror (T425LPXR, Chroma, Bellows Falls, VT). A second pair of lenses is used to focus the light at the back focal plane of the objective after reflection by a dichroic filter (Di-FF506, Semrock, Rochester, NY). Fluorescence images of the samples at 525 ± 15 nm (F525-30; Semrock, Rochester, NY) are acquired with a 10 x fluar (NA 0.5, Carl Zeiss AG, Feldbach, Switzerland) objective. Objectives are mounted on a home-built microscope equipped with a Luca-R CCD camera (Andor Technology, Belfast, UK). The bottom surface of the imaged sample is placed on a 0.4 mm thick copper disk with a hole of 8 mm diameter. This metal holder

is mounted on an aluminum block thermostatted at 20 ± 0.2 °C with two thermoelectric Peltier devices (CP 1.0-63-05 L-RTV; Melcor, Trenton, NJ). The stage temperature is maintained at 20 °C with a TCS610 thermistor (Wavelength Electronics, Bozeman, MT) and the feedback loop is driven by a MPT10000 temperature controller (Wavelength Electronics, Bozeman, MT).

The Dronpa-2 samples are periodically submitted to a constant illumination of intensity I_{480} = 0.326 Ein m^{-2} s^{-1} at 480 nm during 1 s and a constant illumination of intensity I_{405} = 0.06 Ein m^{-2} s^{-1} at 405 nm during 1 s. The GCaMP6s-Q samples are periodically submitted to a constant illumination of intensity $I_{480} = 0.378$ Ein m^{-2} s^{-1} at 480 nm during 1.6 s and a constant illumination of intensity I_{405} = 0.06 Ein m^{-2} s^{-1} at 405 nm during 1.6 s. The calibration of the light intensity is performed following the same protocol as for the fluorimeter.[6, 11]

Each sample is subjected to 5 periods of illumination. The first period is used to erase the history of the sample and discarded. The following four periods are recorded. The acquisition frequency of the camera is set to 500 Hz for Dronpa-2 and 300 Hz for GCaMP6s-Q. The fluorescence evolution of each sample is recorded in a 64 x 64 pixels area with a binning of 2 in order to obtain a 32 x 32 image for each time step.

3 Theory

In this section, we introduce the correlation method, aiming at linking a fluorescence time series associated with a characteristic time to an observable proportional to either the concentration of the fluorophore or the concentration of a species reacting with the flurophore and affecting the characteristic time of fluorescence evolution. The idea is to correlate the fluorescence time series with a weighting function associated with the characteristic time of the target in order to optimize the correlation output. In order to avoid the pollution of the correlation output with possible interfering fluorophores, we will discuss how the correlation output varies with the characteristic time of the weighting function. Weighting functions leading to sharp variations of the correlation output will be preferred in order to improve the accuracy of titration. Subsections 3.1 and 3.2 present the theory for two different scalings leading to an observable proportional to the concentration of the fluorophore and a species reacting with it, respectively.

3.1 Titration of a photoswitchable fluorophore

We define the output $O_\beta(\tau)$ as the correlation between the input time series $I(t)$ and a weighting function $w_{\beta,\tau}(t)$ associated with the characteristic time τ

$$O_\beta(\tau) = \frac{1}{\beta\tau}\int_0^{\beta\tau} I(t)w_{\beta,\tau}(t)\mathrm{d}t \tag{2}$$

where the parameter $\beta > 0$ controls the integration time $\beta\tau$. The input and the output have the same units. Consequently, if the input time series is proportional to the concentration of a

fluorophore, the observable $O_\beta(\tau)$ has the same property and can be used to titrate the targeted fluorophore.

The input time series contains a time-dependent term and a baseline offset B. The output $O_\beta(\tau)$ is independent of B provided that the mean value $\frac{1}{\beta\tau}\int_0^{\beta\tau} w_{\beta,\tau}(t)\mathrm{d}t$ of the weighting function vanishes. This property ensures that any constant contribution to the input time series such as autofluorescence is eliminated by the correlation method. In the following, this condition is assumed to be fulfilled.

In order to evaluate the signal-to-noise ratio associated with the output $O_\beta(\tau)$, we consider the noisy input time series

$$I(t) = f(t) + \epsilon n(t) \tag{3}$$

where $f(t)$ is a deterministic term and $n(t)$, a centered Gaussian white noise of variance n_0 obeying

$$\langle n(t)\rangle = 0 \tag{4}$$

$$\langle n(t_1)n(t_2)\rangle = n_0\delta\left(t_1 - t_2\right) \tag{5}$$

where $\langle . \rangle$ is the mean value. We assume that the noise variance n_0 is constant, which is reasonable in a small range of variation of fluorescence intensity.

The standard deviation $N^I(t)$ associated with the input time series $I(t)$ is given by [24, 25]

$$N^I(t) = \sqrt{\langle I(t)^2\rangle - \langle I(t)\rangle^2} \tag{6}$$

The signal-to-noise ratio $SNR^I(t)$ is evaluated by

$$SNR^I(t) = \left|\frac{\langle I(t)\rangle}{N^I(t)}\right| \tag{7}$$

The considered photoswitchable fluorophores being mostly engaged in first-order light- and thermally-driven reactions, the fluorescence signal evolves as a linear combination of exponential terms.[26] We apply Eq. (7) to a noisy time series $I_\mathrm{m}(t) = f_\mathrm{m}(t) + \epsilon n(t)$, where $f_\mathrm{m}(t)$ is a typical monoexponential function

$$f_\mathrm{m}(t) = A\exp\left(-\frac{t}{\tau_m}\right) + B \tag{8}$$

with the prefactor A and the characteristic time τ_m. We obtain $SNR^{I_\mathrm{m}}(0) = (A+B)/\epsilon\sqrt{n_0}$. The difference $\Delta I_\mathrm{m} = I_\mathrm{m}(t=0) - I_\mathrm{m}(t\to\infty)$ is associated with the signal-to-noise ratio

$$SNR^{\Delta I_\mathrm{m}} = \frac{A}{\epsilon\sqrt{2n_0}} \tag{9}$$

We use Eqs. (6,7) in which $I(t)$ has been replaced by $O_\beta(\tau)$ to estimate the noise and the signal-to-noise ratio associated with the output $O_\beta(\tau)$. According to Eqs. (2-5), we obtain the

output noise

$$N_\beta^O(\tau) = \frac{\epsilon}{\beta\tau}\sqrt{n_0 \int_0^{\beta\tau} w_{\beta,\tau}(t)^2 \mathrm{d}t} \tag{10}$$

and the signal-to-noise ratio

$$SNR_\beta^O(\tau) = \left| \frac{\int_0^{\beta\tau} f(t) w_{\beta,\tau}(t) \mathrm{d}t}{\epsilon\sqrt{n_0 \int_0^{\beta\tau} w_{\beta,\tau}(t)^2 \mathrm{d}t}} \right| \tag{11}$$

The behavior of the output $O_\beta(\tau)$ for 15 different weighting functions is studied. The definition of the weighting functions, labeled from *a* to *o*, is given in Tab. A.1. *A priori*, any weighting function $w_{\beta,\tau}(t)$ associated with a characteristic time τ can be used to compute an output $O_\beta(\tau)$ which behaves as a function of τ. A spectrum $O_\beta(\tau)$ characterizing the photoswitching kinetics described by the input time series $I(t)$ is obtained as the characteristic time τ of the weighting function varies. We consider weighting functions that have been introduced in the literature[15, 16, 17, 18] to tune the properties of the output. Specifically, the integral of the studied weighting functions between 0 and $\beta\tau$ is zero to eliminate the possible offset of the input time series. In addition, the shape of the weighting function is adapted to change the bandwidth of the spectrum $O_\beta(\tau)$. As already mentioned, the bandwidth of the spectrum of characteristic times has an impact on the selectivity of titration. In a mixture of interfering photoswitchable fluorophores, as small as possible bandwidths enable a better discrimination of the targeted fluorophore.

Due to the linearity of integration, the output of a sum of time series is equal to the sum of the outputs of each time series. Hence, applying Eq. (2) to the monoexponential time series without noise given in Eq. (8) is sufficient to discuss the behavior of a multiexponential input time series. For all weighting functions, the output $O_\beta(\tau)$ is proportional to the prefactor A. As shown in Figs. 1a,b, $O_\beta(\tau)$ displays an extremum for a value of τ/τ_m which depends on the parameter β. The output $O_\beta(\tau)$ vanishes when τ is very different from τ_m. Hence the output behaves as a band-pass filter. For each weighting function, the extremum of the output occurs for $\tau = \tau_m$ for a specific β value, denoted β^*. The sharpness of the extremum is characterized by the ratio bandwidth W_{β^*} defined as the ratio of the two times for which the output is equal to half the extremum output. The values of β^*, the scaled output at the extremum, $M = O_{\beta^*}(\tau_m)/A$, and the ratio bandwidth W_{β^*} are given in Tab. A.2 for the monoexponential input time series.

The band-pass behavior of the output can be harnessed to titrate a targeted species associated with a known characteristic time τ_m. Indeed the output $O_{\beta^*}(\tau_m)$ determined at the characteristic time τ_m provides a quantity proportional to the amount of the targeted species. Nevertheless, the method requires the integration over the interval $[0, \beta^*\tau_m]$ which implies that

the acquisition time of the fluorescence input time series has to reach at least $\beta^*\tau_m$. According to Eq. (2), the output associated with a mixture of photoswitching species is the sum of the outputs associated with each single species. Consequently, the titration can be performed without separation provided that the characteristic time of the targeted species τ_m is sufficiently different from the characteristic times τ_n of the other species. Specifically the ratio τ_n/τ_m must be larger than the ratio bandwidth W_{β^*}.

Equation (11) is used to compute the output signal-to-noise ratio $SNR^O_\beta(\tau)$ for $f(t) = f_{\mathrm{m}}(t)$. The signal-to-noise ratio shows a similar behavior as the output $O_\beta(\tau)$. In particular $SNR^O_\beta(\tau)$ is maximum for $\tau = \tau_m$ and $\beta = \beta^*$. In addition, the signal-to-noise ratio $SNR^O_{\beta^*}(\tau)$ is proportional to $\sqrt{\tau}$ for a continuous function of time, implying that the sensitivity to noise of the output decreases as the upper limit of integration increases. Improving the signal-to-noise ratio may imply considering a longer acquisition time.

Relevant properties of the weighting functions $a - o$, i.e. the acquisition time, the signal-to-noise ratio and the sensitivity of the detection of a specific characteristic time, are characterized by the corresponding coordinates in the $(\beta^*, SNR^O_{\beta^*}(\tau_m)\epsilon\sqrt{n_0}/(A\sqrt{\tau_m}), W_{\beta^*})$ space. Figures 1c and 1d show a projection in the $(\beta^*, SNR^O_{\beta^*}(\tau_m)\epsilon\sqrt{n_0}/(A\sqrt{\tau_m}))$ space and the $(SNR^O_{\beta^*}(\tau_m)\epsilon\sqrt{n_0}/(A\sqrt{\tau_m}), W_{\beta^*})$ space, respectively.

For each of the 15 weighting functions $a - o$, Fig. 1c associates the value of β^* with the maximum scaled signal-to-noise ratio $SNR^O_{\beta^*}(\tau_m)$. The values of $SNR^O_{\beta^*}(\tau_m)$ are given in Tab. A.2. Figure 1d associates $SNR^O_{\beta^*}(\tau_m)$ with the ratio bandwidth W_{β^*} for each weighting function. The weighting functions leading to high signal-to-noise ratios are associated with small values of β^* but large ratio bandwidths W_{β^*}. Conversely, the weighting functions leading to low signal-to-noise ratios are associated with large values of β^* but small ratio bandwidths. The asymmetry of the spectrum obtained for β^* mostly increases when switching from one weighting function to another in the order $a, ..., o$.

The previous results can be harnessed as follows in a purpose of discrimination of several photoswitching species associated with known characteristic times. The experimentalist has to find a balance between optimizing the signal-to-noise ratio and the ratio bandwidth, which leads to the choice of an optimal weighting function. The ratio bandwidth can be ignored in the case of the titration of a photoswitching species in the absence of other photoswitching components. In this case, the optimum signal-to-noise ratio and the smallest value of β^*, i.e. the smallest acquisition time, are obtained for the weighting functions a and b.

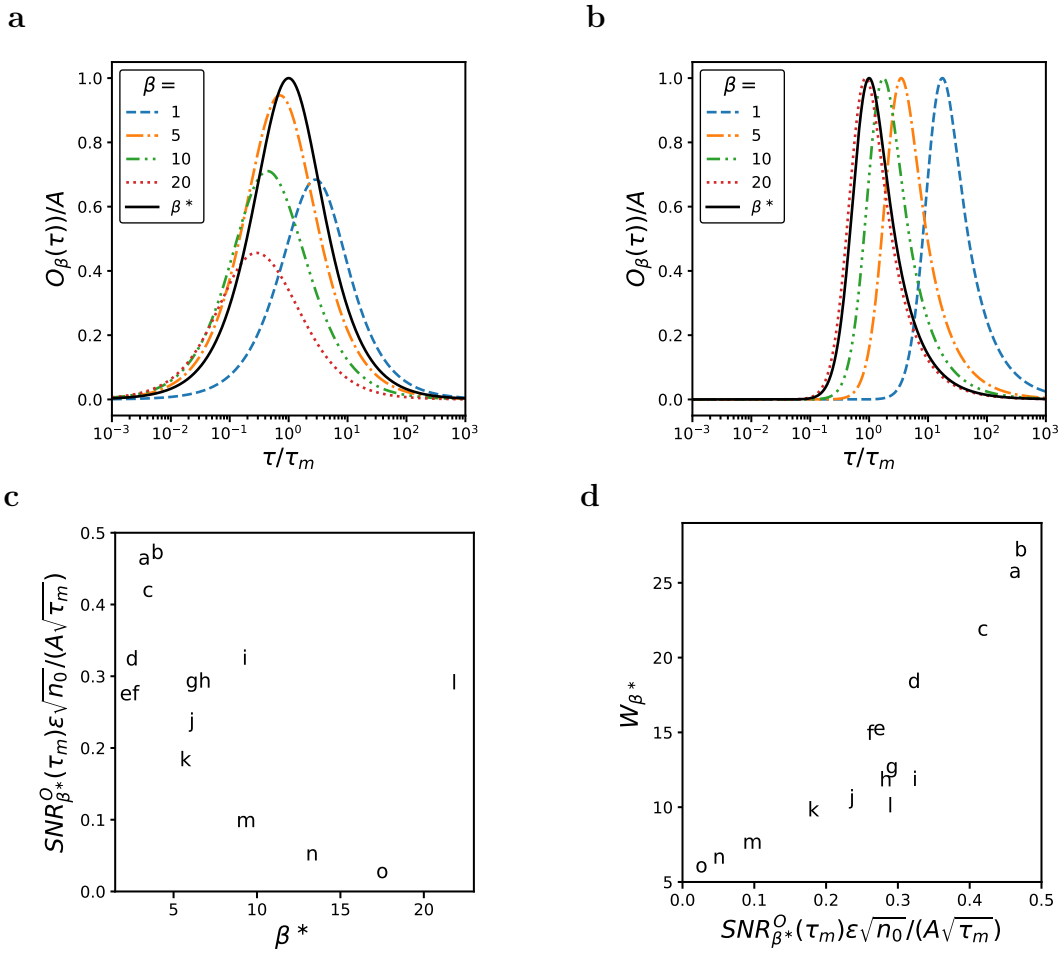

Figure 1: **a**: Output $O_\beta(\tau)/A$ versus τ/τ_m for different values of β for the weighting function a ($\beta^* = 3.245$). **b**: Output $O_\beta(\tau)/A$ versus τ/τ_m for different values of β for the weighting function o ($\beta^* = 17.501$). **c**: The letters $a - o$ are located at the coordinates $(\beta^*, SNR^O_{\beta^*}(\tau_m)\epsilon\sqrt{n_0}/(A\sqrt{\tau_m}))$ computed for the corresponding weighting functions $a - o$. $\beta^*\tau$ is the optimum integration limit and $SNR^O_{\beta^*}(\tau_m)\epsilon\sqrt{n_0}/(A\sqrt{\tau_m})$ is the scaled signal-to-noise ratio. **d**: The letters $a - o$ are located at the coordinates $(SNR^O_{\beta^*}(\tau_m)\epsilon\sqrt{n_0}/(A\sqrt{\tau_m}), W_{\beta^*})$ computed for the corresponding weighting functions $a - o$. W_{β^*} is the ratio bandwidth of the output $O_{\beta^*}(\tau)$.

3.2 Titration of a species reacting with the photoswitchable fluorophore

The kinetic properties of a photoswitchable fluorophore can be harnessed to titrate a non fluorescent species which reacts with the fluorophore and induces a change in the fluorescence evolution. The characteristic times associated with the fluorescence dynamics depend on the concentration of the targeted non fluorescent species. In this context, a relevant observable should extract the kinetic information which gives access to the concentration of the titrated species regardless of the amount of fluorophore.

The output $O_\beta(\tau)$ defined in Eq. (2) scales as the input time series $I(t)$. In the case of fluorescence intensity, $O_\beta(\tau)$ is proportional to the concentration and the brightness of the fluorophore, the light intensity, and the setup characteristics. In order to eliminate this dependence, we define a scaled output as

$$\Omega_\beta(\tau) = \frac{O_\beta(\tau)}{\sigma_I \sigma_w} \tag{12}$$

where $O_\beta(\tau)$ is given in Eq. (2). The standard deviations of the input time series and the weighting function are

$$\sigma_I = \sqrt{\frac{1}{\beta\tau}\int_0^{\beta\tau} \left(I(t)-\mu_I\right)^2 \mathrm{d}t} \tag{13}$$

$$\sigma_w = \sqrt{\frac{1}{\beta\tau}\int_0^{\beta\tau} w_{\beta,\tau}(t)^2 \mathrm{d}t} \tag{14}$$

where $\mu_I = \frac{1}{\beta\tau}\int_0^{\beta\tau} I(t)\mathrm{d}t$ is the mean value of the input $I(t)$ and $\beta > 0$.

Similarly to $O_\beta(\tau)$, the scaled output $\Omega_\beta(\tau)$ is independent of the baseline offset of the input time series if $\frac{1}{\beta\tau}\int_0^{\beta\tau} w_{\beta,\tau}(t)\mathrm{d}t = 0$.

The noisy input time series given in Eq. (3) where the Gaussian white noise $n(t)$ of variance n_0 obeys Eqs. (4,5) is used to calculate the signal-to-noise ratio. Performing an expansion in $\epsilon \ll 1$ and using Eq. (6), we find that the scaled output noise is

$$N_\beta^\Omega(\tau) = \frac{\epsilon}{\sigma_f}\sqrt{\frac{n_0}{\beta\tau}\left(1-\frac{a^2}{\sigma_f^2\sigma_w^2}\right)} \tag{15}$$

where $\sigma_f = \sqrt{\frac{1}{\beta\tau}\int_0^{\beta\tau}(f(t)-\mu_f)^2\mathrm{d}t}$, $\mu_f = \frac{1}{\beta\tau}\int_0^{\beta\tau} f(t)\mathrm{d}t$, $a = \frac{1}{\beta\tau}\int_0^{\beta\tau} f(t)w_{\beta,\tau}(t)\mathrm{d}t$, and σ_w is given in Eq. (14). Equation (15) holds for all the weighting functions $w_{\beta,\tau}(t)$. The time series $f(t) = I(t) - \epsilon n(t)$ is the deterministic part of the input time series. The signal-to-noise ratio reads

$$SNR_\beta^\Omega(\tau) = \frac{a\sqrt{\beta\tau}}{\sigma_w \epsilon \sqrt{n_0\left(1-\frac{a^2}{\sigma_f^2\sigma_w^2}\right)}} \tag{16}$$

As in the previous subsection, the scaled output $\Omega_\beta(\tau)$ is calculated using the monoexponential input time series of characteristic time τ_m and prefactor A given in Eq. (8) for the 15 weighting functions given in Tab. A.1. It is worth noting that, due to the chosen scaling, the output is not a linear function of the input.

The scaled output $\Omega_\beta(\tau)$ is independent of the absolute prefactor A but has the sign of A. The variation of the scaled output $\Omega_\beta(\tau)$ with τ/τ_m depends on the weighting function. Three types of behaviors are observed. $\Omega_\beta(\tau)$ displays an extremum and a non vanishing limit as $\tau/\tau_m \to 0$ for the weighting functions a, b, and c, as shown in Fig. 2a. $\Omega_\beta(\tau)$ monotonously evolves and has an inflection point for the weighting functions d, e, and f, as illustrated in Fig. 2b. $\Omega_\beta(\tau)$ shows an extremum and vanishing limits as $\tau/\tau_m \to 0$ and $\tau/\tau_m \to \infty$ for the weighting functions g - o, as displayed in Fig. 2c. The argument τ/τ_m of the extremum or the inflection point depends on the parameter β. For the weighting functions associated with an extremum of $\Omega_\beta(\tau)$, the extremum occurs for $\tau = \tau_m$ for a specific value β^*, except for the weighting function a for which $\Omega_\beta(\tau_m)$ is extremum for all β values. Due to the lack of extremum of $\Omega_\beta(\tau)$ for the weighting functions $d - f$, no β^* value can be defined in these cases. The values of $\lim_{\tau\to 0}|\Omega_\beta(\tau)|$, the optimum parameter β^*, the scaled output at the extremum $|\Omega_{\beta^*}(\tau_m)|$, and the ratio bandwidth W_{β^*} of $\Omega_{\beta^*}(\tau)$ are given in Tabs. A.3, A.5, A.6.

We compute the signal-to-noise ratio $SNR^\Omega_\beta(\tau)$ given in Eq. (16) for the monoexponential input time series given in Eq. (8). For the weighting function a, the scaled output noise given in Eq. (15) vanishes for $\tau = \tau_m$. Consequently, the signal-to-noise ratio diverges at leading order. The signal-to-noise ratio $SNR^\Omega_\beta(\tau)$ is numerically computed using a statistics over 10000 monoexponential decays of characteristic time τ_m and prefactor A with an additive Gaussian white noise of standard deviation $\epsilon\sqrt{n_0}$. The following values of the parameters $(\tau_m, \epsilon\sqrt{n_0}/A) = (1, 0.01)$, $(1, 0.05)$, $(1, 0.1)$, $(0.2, 0.1)$, $(5, 0.1)$ are considered. The time range of the input time series is equal to 50 and the sampling time is $t_s = 0.01$. For each decay, the scaled output $SNR^\Omega_\beta(\tau_m)$ is computed according to Eq. (12) with a β value ranging from 1 to 20. For each value of τ_m/t_s and $\epsilon\sqrt{n_0}/A$, the variation of the signal-to-noise ratio $SNR^\Omega_\beta(\tau_m)$ with β is determined. We find that the scaled signal-to-noise ratio $SNR^\Omega_\beta(\tau_m)\epsilon^2 n_0/(A^2\sqrt{\tau_m/t_s})$ displays a maximum for $\beta = \beta^\dagger$ as shown in Fig. A.1.

For the weighting functions $b - o$, the analytical prediction given in Eq. (16) is used to calculate the signal-to-noise ratio $SNR^\Omega_\beta(\tau)$ for the monoexponential input time series given in Eq. (8). For a specific value $\beta^\dagger$, the signal-to noise ratio displays a maximum for $\tau = \tau_m$. For the weighting functions b, c, $g - o$, the scaled output $\Omega_{\beta^\dagger}(\tau)$ is extremum for the characteristic time $\tau^\dagger$. The values of $\beta^\dagger$, the value $M = |\Omega_{\beta^\dagger}(\tau_m)|$, the ratio bandwidth $W_{\beta^\dagger}$ of $\Omega_{\beta^\dagger}(\tau)$, and the characteristic time $\tau^\dagger$ are given in Tabs. A.4, A.5, A.7. The signal-to-noise ratios $SNR^\Omega_{\beta^*}(\tau_m)$ and $SNR^\Omega_{\beta^\dagger}(\tau_m)$ are also given in Tabs. A.3–A.7. The scaled outputs evaluated for β^* and $\beta^\dagger$

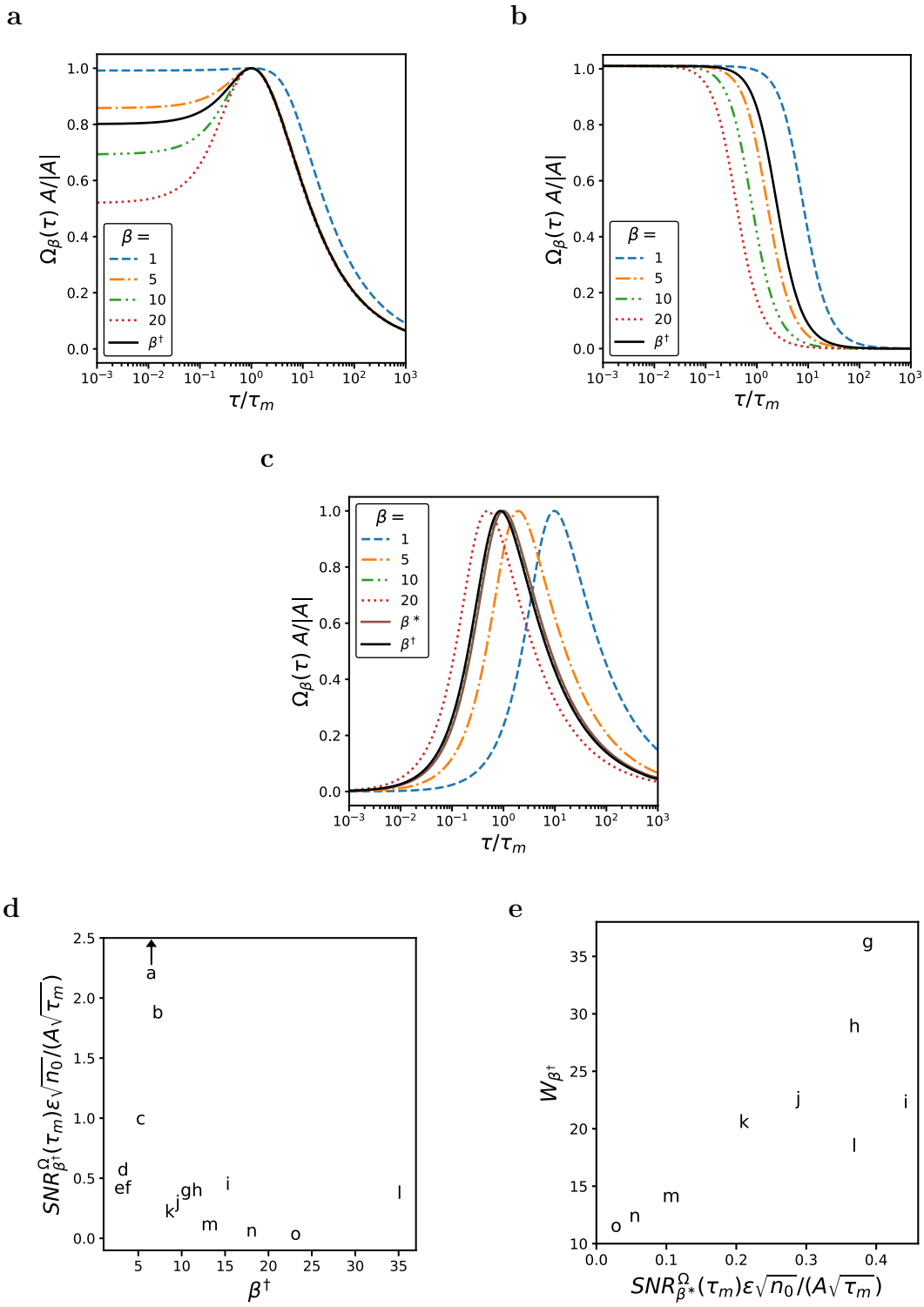

Figure 2: **a**: Scaled output $\Omega_\beta(\tau)$ versus τ/τ_m for different values of β for the weighting function a ($\beta^\dagger = 6.5$). **b**: Scaled output $\Omega_\beta(\tau)$ versus τ/τ_m for different values of β for the weighting function d ($\beta^\dagger = 3.247$). **c**: Scaled output $\Omega_\beta(\tau)$ versus τ/τ_m for different values of β for the weighting function g ($\beta^* = 9.74$, $\beta^\dagger = 11.15$). **d**: The letters $a-o$ are located at the coordinates $(\beta^\dagger, SNR^{\Omega}_{\beta^\dagger}(\tau_m)\epsilon\sqrt{n_0}/(A\sqrt{\tau_m}))$ computed for the corresponding weighting functions $a-o$. $\beta^\dagger\tau$ is the optimum integration limit and $SNR^{\Omega}_{\beta^\dagger}(\tau_m)\epsilon\sqrt{n_0}/(A\sqrt{\tau_m})$ is the scaled signal-to-noise ratio. **e**: The letters $g-o$ are located at the coordinates $(SNR^{\Omega}_{\beta^\dagger}(\tau_m)\epsilon\sqrt{n_0}/(A\sqrt{\tau_m}), W_{\beta^\dagger})$ computed for the corresponding weighting functions $g-o$. $W_{\beta^\dagger}$ is the ratio bandwidth of the scaled output $\Omega_{\beta^\dagger}(\tau)$.

have similar properties, which means that the limits of integration, such that the observable and the signal-to-noise ratio are maximum for the targeted charateristic time, are close. Either β^* or $\beta^\dagger$ can be chosen to compute the scaled output.

For each weighting function $a-o$, the acquisition time and the signal-to-noise ratio are characterized by the corresponding coordinates in the $(\beta^\dagger, SNR^\Omega_{\beta^\dagger}(\tau_m)\epsilon\sqrt{n_0}/(A\sqrt{\tau_m}))$ space, as shown in Fig. 2d. For the weighting functions $g-o$ which lead to an extremum of the scaled output, the signal-to-noise ratio and the sensitivity of the detection of a specific characteristic time are also characterized by their coordinates in the $(SNR^\Omega_{\beta^\dagger}(\tau_m)\epsilon\sqrt{n_0}/(A\sqrt{\tau_m}), W_{\beta^\dagger})$ space, as displayed in Fig. 2e. The signal-to-noise ratio of the weighting function a is much larger than the signal-to-noise ratios of the other weighting functions since the first order of the expansion with respect to ϵ diverges for a. In addition, the weighting functions $a-f$ associated with high signal-to-noise ratios and small values of $\beta^\dagger$ lead to low-pass filters for the scaled outputs $\Omega_{\beta^\dagger}(\tau)$. The weighting functions $g-o$ leading to band-pass filters for $\Omega_{\beta^\dagger}(\tau)$ are associated with low signal-to-noise ratios and large values of $\beta^\dagger$. In this case, a small bandwidth $W_{\beta^\dagger}$ is associated with a low signal-to-noise ratio.

If the fluorophore is the single photoswitching species in the solution, the best weighting function is the exponential function a leading to the best signal-to-noise ratio and a scaled output nearly independent of the parameter β, i.e. a small integration time. If the goal is to discriminate between several photoswitchable fluorophores, the scaled output must behave as a band-pass filter observed for the weighting functions $g-o$ which requires a large value of β and imposes a small signal-to-noise ratio. A balance has to be found between the signal-to-noise ratio and the ratio bandwidth. The weighting function g will be preferred when the ratio bandwidth is not limiting. Conversely the weighting function o will be chosen when photoswitching species with very close characteristic times interfere.

4 Experimental validation and applications

In this section we report on experiments in order to validate the properties of the spectra of characteristic times predicted for a theoretical monoexponential input time series. We select two photoswitching fluorophores, the reversibly photoswitchable fluorescent protein Dronpa-2 and the reversibly photoswitchable calcium sensor GCaMP6s-Q, which displays a fluorescence evolution sufficiently close to an exponential function under constant illumination. Dronpa-2 illustrates the application of the correlation method to the titration of a fluorescent species and GCaMP6s-Q is used to titrate a species, namely calcium, reacting with the fluorophore.

4.1 Titration of the photoswitchable fluorophore Dronpa-2

Under illumination at 480 nm, Dronpa-2 is known to switch from a bright state to a dark state, leading to a decrease of fluorescence. The bright state is recovered using illumination at 405 nm.

Several Dronpa-2 solutions in phosphate saline buffer (PBS = $[NaH_2PO_4] = 10$ mM, $[Na_2HPO_4] = 40$ mM, $[NaCl] = 150$ mM in H_2O, pH 7.4) at different concentrations are illuminated at the wavelength 480 nm ($I_{480} = 4.5\ 10^{-3}$ Ein m^{-2} s^{-1}) and their fluorescence is recorded as shown in Figs. 3a and SI-1. Equation (1) is used to obtain the time $\tau_m = 1.13$ s characterizing the fluorescence time series.

The fluorescence time series are processed using Eq. (2) and we compute the outputs $\overline{O_x}(\tau) = O_{\beta^*}(\tau)/M$ for the weighting functions $x = a, d, g, k, o$ with the appropriate β^* value. The scaling factor M, given in Tab. A.2, is calculated using the monoexponential input time series given in Eq. (8) and for each weighting function x. By construction, the scaling is chosen to ensure that the maximum of $\overline{O_x}(\tau)$ is equal to the prefactor A for a monoexponential input time series.

As shown in Figs. 3b and SI-2, the outputs $\overline{O_x}(\tau)$, for $x = a, d, g, k, o$, display a maximum for a characteristic time τ close to $\tau_m = 1.13$ s regardless of the concentration of Dronpa-2. The values of the outputs at the extremum are also close to the pre-exponential factor A of the input time series given in Fig. 3a. The experimental ratio bandwidth is 14% to 24% smaller than the theoretical prediction W_{β^*} depending on the weighting function. This deviation originates from the small minimum around $\tau_n = 0.1$ s observed in Fig. 3b which may reveal the presence of a second characteristic time τ_n. However, the prefactor associated with τ_n is much smaller than the prefactor A associated with τ_m, and the resulting perturbation of the maximum of $\overline{O_x}(\tau)$ is negligible.

Figure 3c displays the linear increase of the maximum output $\overline{O_x}(\tau_m)$ for $x = a, d, g, k, o$ evaluated at $\tau = \tau_m$ as the concentration of the solution of Dronpa-2 increases. This result validates the definition of the observable $\overline{O_x}(\tau_m)$ for titration purposes. The corresponding input time series are displayed in Fig. SI-1. For each concentration of Dronpa-2, the data points corresponding to the different weighting functions are superimposed proving that any weighting function can be chosen to provide the concentration of Dronpa-2.

We now investigate the sensitivity of the correlation method to noise. To this goal, we analyze the spatial dependence of images of the fluorescence of a solution of Dronpa-2 at 0.12 μM, in PBS buffer pH 7.4 injected in an 80 μm thick coverslip chamber and illuminated at 480 nm ($I_{480} = 0.326$ Ein.m^{-2}.s^{-1}). Fluorescence is recovered using illuminations at 405 nm between three successive illuminations at 480 nm. The fluorescence evolution averaged over the region of interest remains nearly unchanged when considering any of the three illuminations at

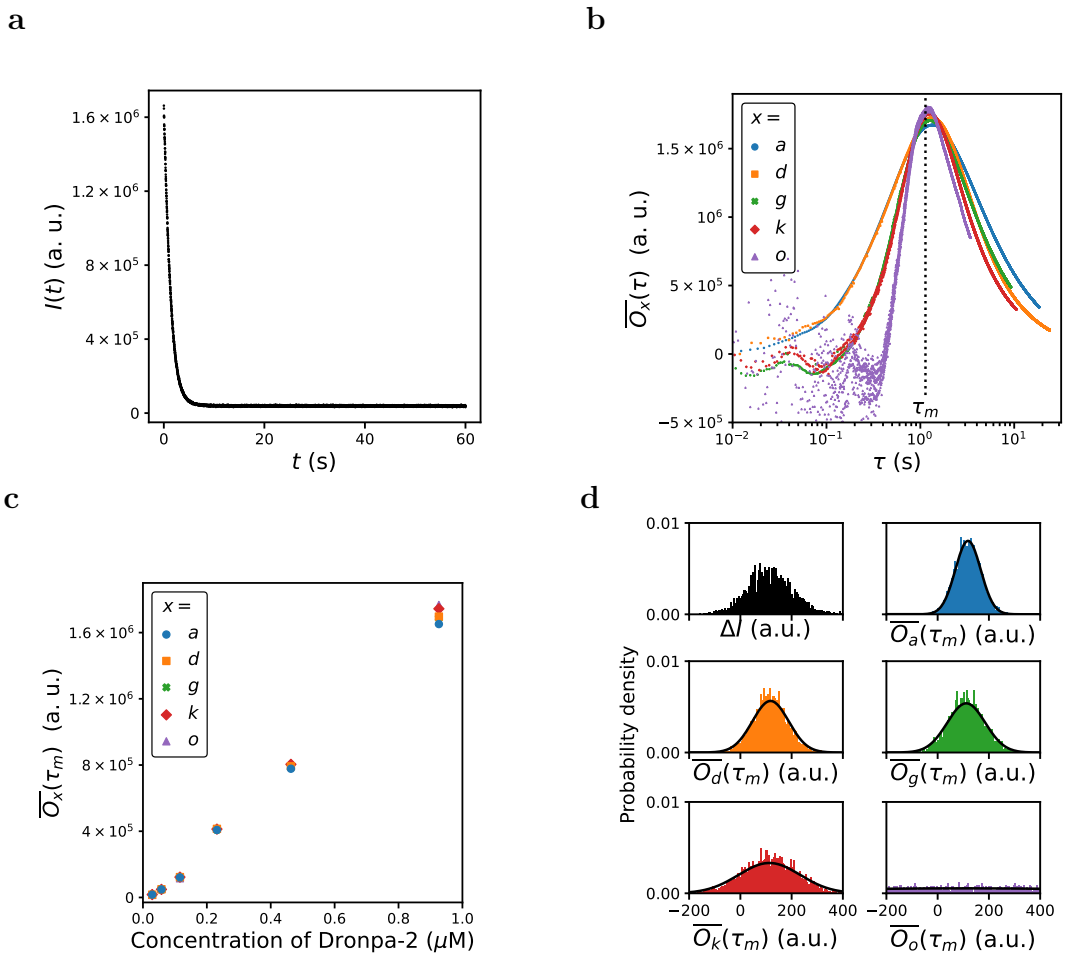

Figure 3: **a**: Fluorescence time series of a solution of Dronpa-2 ([Dronpa-2] = 0.93 μM in PBS buffer at pH 7.4) under illumination at 480 nm (I_{480} = 4.51 10^{-3} Ein m^{-2} s^{-1}) recorded at 515 nm. **b**: Outputs $\overline{O_x}(\tau)$ obtained for the input time series given in subfigure **a** versus characteristic time τ for the weighting functions $x = a, d, g, k, o$. **c**: Outputs $\overline{O_x}(\tau_m)$ versus concentration of the solution of Dronpa-2 for the weighting functions $x = a, d, g, k, o$. **d**: Histograms of $\Delta I = I(0) - I(\infty)$ (black) and the outputs $\overline{O_x}(\tau_m)$ for $x = a$ (blue), $x = d$ (orange), $x = g$ (green), $x = k$ (red), and $x = o$ (purple) deduced from the 3072 time series. The black solid lines are the Gaussian distributions of mean $\langle\overline{O_x}(\tau_m)\rangle$ and standard deviations $\langle\overline{O_x}(\tau_m)\rangle SNR^{\overline{O_x}}(\tau_m)$ predicted by the theoretical analysis. The input and outputs are expressed in the same arbitrary units.

480 nm, as shown in Fig. SI-3. We divide the region of interest in 32×32 pixels (pixel size: 1.02 μm) and perform a statistical analysis using the three illuminations at 480 nm and the 32×32 pixels leading to 3072 time series $I(t)$. Equation (1) is used to obtain the characteristic time

$$\tau_m = 0.0157 \text{ s} \tag{17}$$

at the chosen light intensity.

For each of the 3072 time series $I(t)$, we apply Eqs. (6, 7) to $\Delta I = I(0) - I(\infty)$, where $I(\infty)$ is the value of the fluorescence intensity associated with the largest recorded time. Since the time series $I(t)$ behaves as the monoexponential function $I_{\mathrm{m}}(t)$, we use Eq. (9) to estimate the signal-to-noise ratio $A/\epsilon\sqrt{2n_0}$ of the quantity ΔI. The histogram of ΔI is shown in Fig. 3d. We find

$$\frac{A}{\epsilon\sqrt{n_0}} = 1.84 \tag{18}$$

The outputs $\overline{O_x}(\tau)$ are calculated for each of the 3072 time series $I(t)$ and the weighting functions $x = a, d, g, k, o$. Satisfactorily, $\overline{O_x}(\tau)$ reaches a maximum for τ close to the expected value $\tau_m = 0.0157$ s. Figure 3d displays the histograms of the distributions of $I(0) - I(\infty)$ and the outputs $\overline{O_x}(\tau_m)$ for $x = a, d, g, k, o$. We estimate the mean output $\langle\overline{O_x}(\tau_m)\rangle$ and the output signal-to-noise ratio by applying Eqs. (6, 7) for $I(t)$ replaced by $\overline{O_x}(\tau_m)$. Due to noise, some input time series take increasing values instead of the expected decreasing values, leading to negative outputs. The signal-to-noise ratio associated with the output $\overline{O_x}(\tau)$ for the weighting function x is denoted by $SNR^{\overline{O_x}}(\tau)$.

The scaled output signal-to-noise ratios $SNR^{\overline{O_x}}(\tau_m)\epsilon\sqrt{n_0}/(A\sqrt{\tau_m})$ predicted for a monoexponential input time series are given in Tab. A.2. The comparison with the experimental results requires to take into account the normalization factors $A/\epsilon\sqrt{n_0}$ given in Eq. (18) and the characteristic time τ_m given in Eq. (17). For discrete times, the noise is known to scale as the square root of the sampling time t_s.[24, 27] Consequently, the characteristic time τ_m has to be scaled by the sampling time $t_s = 0.002$ s before comparing the experimental signal-to-noise ratio with the result obtained for a continuous theoretical description. The probability density functions of the normal laws of mean value $\langle\overline{O_x}(\tau_m)\rangle$ and standard deviations $\langle\overline{O_x}(\tau_m)\rangle SNR^{\overline{O_x}}(\tau_m)$ are successfully compared to the experimental normalized histograms in Fig. 3d. The experimental output signal-to-noise ratios and the values predicted for the monoexponential input time series lead to a very satisfying relative deviation of around 8%. The excellent match between the experimental and predicted results validates the approach.

To sum up, the output is proportional to the concentration of the RSFP Dronpa-2. The quantity ΔI contains the same information with a poorer signal-to-noise ratio than the outputs

obtained for the weighting functions a, d, g. Contrary to ΔI which is not selective, the correlation method can be used to discriminate several photoswitching fluorophores in a mixture. In addition, the signal-to-noise ratio of the output improves for a larger characteristic time τ_m of the target.

4.2 Titration of calcium reacting with a photoswitchable sensor

Illumination at the wavelength 480 nm drives the photoswitching of GCaMP6s-Q between states of different brightnesses while illumination at the wavelength 405 nm induces the reverse reaction. The brightnesses of the calcium-bound sensor and calcium-free sensor are different. Interestingly, the fluorescence decreases for the calcium-bound sensor and increases for the calcium-free sensor under illumination at 480 nm. Conversely, the fluorescence increases for the calcium-bound sensor and decreases for the calcium-free sensor under illumination at 405 nm.

We submitted a 1 μM GCaMP6s-Q solutions at different concentrations of Ca^{2+} free in 100 mM KCl, 30 mM MOPS (3-(N-morpholino)propanesulfonic acid) pH = 7.2 contained in an 80 μm thick coverslip chamber to four successive illuminations at 480 nm (I_{480} = 0.378 Ein m^{-2} s^{-1}) separated by illuminations at 405 nm to recover fluorescence. The fluorescence evolution under illuminations at 480 nm is recorded. The fluorescence evolution obtained for twelve different concentrations of calcium during the second illumination at 480 nm and averaged over the whole region of interest is shown in Fig. 4a. The fluorescence time series are processed using Eq. (12) and the weighting functions $x = a, d, g, k, o$ with the appropriate $\beta^\dagger$ value. In the following, $\overline{\Omega_x}(\tau)$ denotes the scaled output $\Omega_{\beta^*}(\tau)/M$ for the weighting function x. The scaling factor M, given in Tabs. A.4, A.5, A.7, is calculated using the monoexponential input time series given in Eq. (8) and for each weighting function x. By construction, the scaling is chosen to ensure that the maximum of $|\overline{\Omega_x}(\tau)|$ is equal to 1 for a monoexponential input time series.

The spectra of characteristic times obtained for different concentrations of calcium provide information that can be harnessed to build a titration curve. Specifically, a characteristic time associated with a large monotonous variation of the output as the calcium concentration increases can be exploited. For example, a characteristic time associated with an extremum of the spectrum can be chosen. The scaled outputs $\overline{\Omega_x}(\tau)$ corresponding to each calcium concentration are displayed in Fig. 4b for the weighting function a and Fig. SI-4 for the weighting functions d, g, k, o. For all weighting functions x, the scaled output $\overline{\Omega_x}(\tau)$ has a maximum for high enough calcium concentration ($[Ca^{2+}] \geq 57$ nM) and the fluorescence evolution shown in Fig. 4a initially decreases. For low enough calcium concentration ($[Ca^{2+}] \leq 81$ nM) the scaled output $\overline{\Omega_x}(\tau)$ displays a minimum and the fluorescence evolution increases. The rich properties of the spectra give access to two characteristic times for which the outputs evolve differently

with the calcium concentration, leading to two different titration curves. The following procedure is adopted to determine the two characteristic times. For all calcium concentrations leading to a maximum of $\overline{\Omega_a}(\tau)$, the average argument of the maximum is computed leading to the characteristic time $\tau_m^{\uparrow} = 27.6$ ms. For all calcium concentrations leading to a minimum of $\overline{\Omega_a}(\tau)$, the average argument of the minimum is computed leading to the characteristic time $\tau_m^{\downarrow} = 122$ ms, as shown in Fig. 4b. According to Fig. SI-4, the characteristic time $\tau_m^{\uparrow}$ ($\tau_m^{\downarrow}$, resp.) computed for the weighting function a is close to the average maxima (minima, resp.) of the scaled outputs $\overline{\Omega_x}(\tau)$ for the weighting functions d, g, k, o. Due to the too small acquisition time of fluorescence evolution, the minima of $\overline{\Omega_o}(\tau)$ are not reached. We use the largest accessible time, 71.6 ms, to compute $\overline{\Omega_o}(\tau_m^{\downarrow})$. It is worth noting that the range of characteristic times of a spectrum is limited by the experimental sampling time and the acquisition time.

Figure 4c displays the variation of the scaled outputs $\overline{\Omega_x}(\tau_m^{\uparrow})$ and $\overline{\Omega_x}(\tau_m^{\downarrow})$ versus calcium concentration for the two weighting functions a and k, leading to a monotonous increase and exploitable titration curves. The weighting functions d, g, o lead to similar results as shown in Fig. SI-5. The Hill function $a/(1 + (K/[Ca^{2+}])^{\nu} + b$ is fitted to the titration curves $\overline{\Omega_x}(\tau_m^{\uparrow})$ and $\overline{\Omega_x}(\tau_m^{\downarrow})$ for the weighting functions $x = a, d, g, k, o$. The fitted parameters, i.e. the characteristic concentration K and the Hill coefficient ν, are given in Tabs. SI-1 and SI-2. The characteristic concentration K corresponds to the calcium concentration associated with the half variation of the scaled output between the saturated solution and the calcium-free solution. The steepness of the titration curve is proportional to the Hill coefficient ν at the characteristic concentration K. Depending on the weighting function x, the fitted characteristic concentration K varies from 60.9 nM to 71.6 nM for the characteristic time $\tau_m^{\uparrow}$ and from 69.3 nM to 89.9 nM for the characteristic time $\tau_m^{\downarrow}$. We conclude that K does not sensitively depend on the weighting function but increases when switching from $\tau_m^{\uparrow}$ to $\tau_m^{\downarrow}$. The fitted Hill coefficient ν is close to 4.7 for the characteristic time $\tau_m^{\uparrow}$ and all weighting functions. It ranges from 4.13 to 2.75 from the characteristic time $\tau_m^{\downarrow}$. Hence, the user is led to choose the characteristic time $\tau_m^{\uparrow}$ to build steep titration curves in order to assign the presence or the absence of calcium in a sample. Otherwise, the user is incited to choose the characteristic time $\tau_m^{\downarrow}$ in order to sensitively estimate the amount of calcium.

We analyze the dependence of the scaled output on noise. The experimental results are used to perform a statistical analysis using the three last illuminations at 480 nm and the 32×32 pixels (pixel size: 1.02 μm) leading to similar 3072 time series $I(t)$ shown in Figs. SI-6 and SI-7. The impact of noise is illustrated for the solution of GCaMP6s-Q saturated in calcium. Using Eqs. (6, 7, 9) for $\Delta I = I(0) - I(\infty)$ we estimate $A/\epsilon\sqrt{n_0} = 11.2$.

The outputs $\overline{\Omega_x}(\tau_m^{\uparrow})$ are calculated for each of the 3072 time series $I(t)$ and the weighting functions $x = a, d, g, k, o$. Equations (6, 7) are used to estimate the mean scaled output

$\langle\overline{\Omega_x}(\tau_m^{\uparrow})\rangle$ and the scaled output signal-to-noise ratio. The mean scaled output $\langle\overline{\Omega_x}(\tau_m^{\uparrow})\rangle$ is close to 1 for the calcium-saturated solution as expected. The scaled output signal-to-noise ratios $SNR_{\beta^\dagger}^{\overline{\Omega_x}}(\tau_m^{\uparrow})\epsilon\sqrt{n_0}/(A\sqrt{\tau_m^{\uparrow}})$ predicted for a monoexponential input time series are given in Tabs. A.4, A.5, A.7. The normalization factors $A/\epsilon\sqrt{n_0} = 11.2$ and $\tau_m^{\uparrow} = 27.6$ ms are used to compare the predictions with the experimental results. The characteristic time $\tau_m^{\uparrow}$ is scaled by the sampling time $t_s = 3.33$ ms.[24, 27] The experimental normalized histograms and the probability density functions of the normal laws of mean value $\langle\overline{\Omega_x}(\tau_m^{\uparrow})\rangle$ and standard deviations $\langle\overline{\Omega_x}(\tau_m^{\uparrow})\rangle SNR_{\beta^\dagger}^{\overline{\Omega_x}}(\tau_m^{\uparrow})$ are shown in Fig. 4d. The experimental standard deviations are smaller than the theoretical predictions due to the failure of the monoexponential hypothesis about the input time series. Applying the correlation method to experimental time series leads to better signal-to-noise ratios than expected. In particular, the weighting function a provides an excellent signal-to-noise ratio. The application of the correlation method to the calcium sensor proves that multiexponential time series can be successfully processed using the scaled output.

The determination of the relative fluorescence variation $\Delta I/I(0)$ leads to a satisfying titration curve of calcium using the calcium sensor GCaMP6s-Q as shown in section B.1 and Fig. B.1.[23, 20] Specifically, the fitted characteristic concentration and the fitted Hill coefficient are comparable to the corresponding values associated with the scaled output of the correlation method. As displayed in Fig. 4d, the signal-to-noise ratio is close to the value obtained for the weighting function k, i.e. much smaller than for a. However, $\Delta I/I(0)$ does not depend on the characteristic times of the input time series, but only on the ratio of the prefactor and the baseline offset. As a consequence $\Delta I/I(0)$ does not sensitively vary with the kinetics of the targeted fluorophore. Moreover $\Delta I/I(0)$ may be polluted by both photoswitching and non photoswitching species that contribute to $I(0)$.

5 Conclusion

In this article, the titration of a target species in a mixture without separation is addressed using post-acquisition data processing of time series associated with the fluorescence evolution of photoswitching species. We optimize two versions of a data processing method based on the correlation of an exponential input time series with a weighting function. The two versions differ by the choice of the scaling factor. For both versions, a spectrum of characteristic times is generated by varying the characteristic time of the weighting function and the upper integration limit of the correlation output. The extrema of the spectrum provide information on the dynamics underlying the input time series. Fifteen different weighting functions leading to different shapes of the spectrum of characteristic times have been studied. The upper integration limit of the correlation output has been chosen to either match the argument of an extremum with a characteristic time of the input time series or optimize the signal-to-noise ratio. Inter-

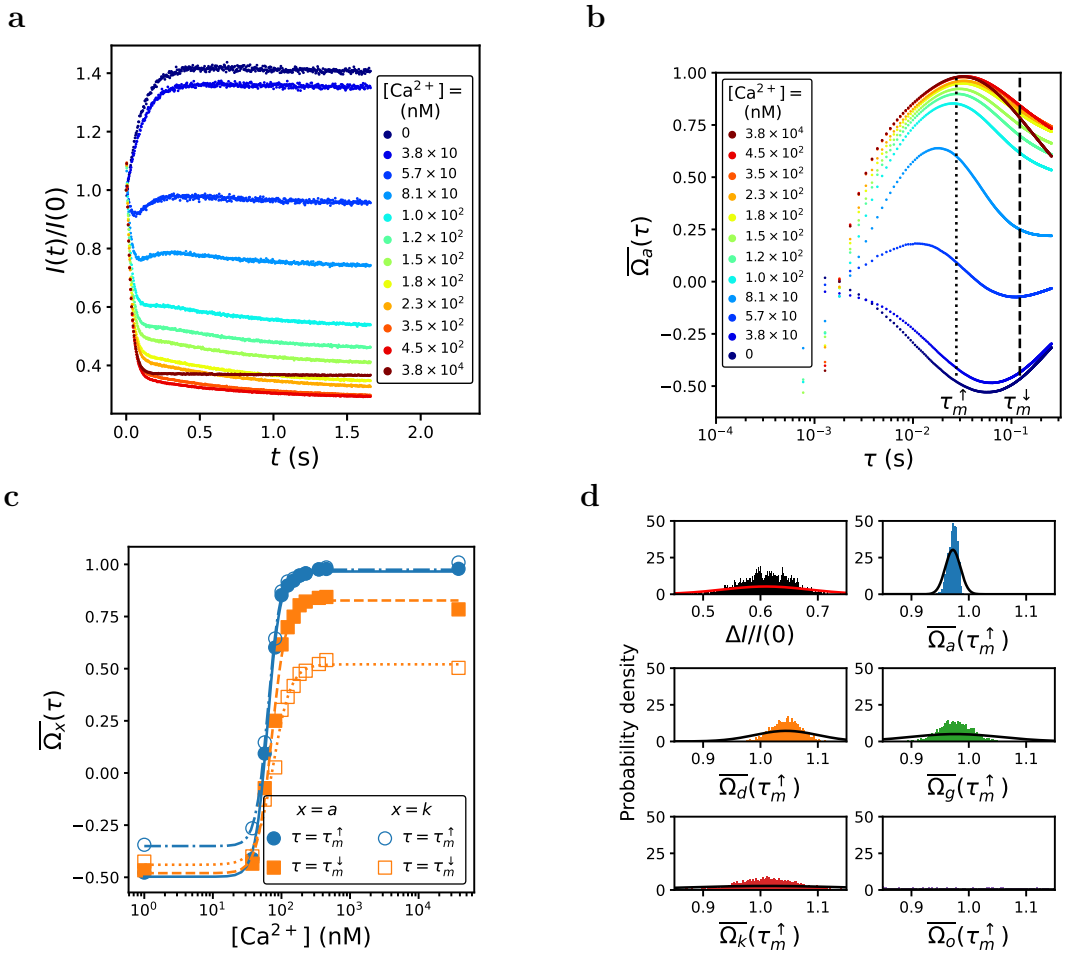

Figure 4: **a**: Fluorescence time series of solutions of the calcium sensor GCaMP6s-Q for different concentrations of Ca^{2+} ([GCaMP6s-Q] = 1 μM in 100 mM KCl, 30 mM MOPS in H_2O, pH = 7.2, 20 °C). The free [Ca^{2+}] of each sample is controlled by the ratio [CaEGTA]/[EGTA].) under illumination at 480 nm (I_{480} = 0.378 Ein m^{-2} s^{-1}) recorded at 515 nm. **b**: Scaled outputs $\overline{\Omega_a}(\tau)$ obtained for the input time series given in subfigure **a** versus characteristic time τ for the weighting function a and different calcium concentrations. **c**: Titration curves $\overline{\Omega_x}(\tau)$ versus calcium concentration [Ca^{2+}] for the weighting functions $x = a, k$ and the characteristic times $\tau = \tau_m^{\uparrow}, \tau_m^{\downarrow}$. The lines give the fitted Hill functions to the experimental results (symbols). **d**: Histograms of $\Delta I/I(0)$ (black) and the scaled outputs $\overline{\Omega_x}(\tau_m^{\uparrow})$ for $x = a$ (blue), $x = d$ (orange), $x = g$ (green), $x = k$ (red), and $x = o$ (purple) deduced from the 3072 time series. The black (red, resp.) solid lines are the Gaussian distributions of mean $\langle\overline{\Omega_x}(\tau_m^{\uparrow})\rangle$ ($\langle\Delta I/I(0)\rangle$, resp.) and standard deviations $\langle\overline{\Omega_x}(\tau_m^{\uparrow})\rangle SNR_{\beta\dagger}^{\overline{\Omega_x}}(\tau_m^{\uparrow})$ ($\langle\Delta I/I(0)\rangle SNR^{\frac{\Delta I}{I(0)}}$, resp.) predicted by the theoretical analysis for the calcium-saturated solution.

estingly, the two values of the integration limit are very close. We select the weighting function leading to the highest possible signal-to-noise ratio compatible with a small enough bandwidth of the spectrum in order to neglect the fluorescence of interfering photoswitchable fluorophores. These results are deduced from the theoretical analysis of a monoexponential input time series but applied to experimental time series that may be more complex.

In a first application, the titration of a photoswitching species is illustrated using the reversibly photoswitchable fluorescent protein Dronpa-2.[22, 28] The spectrum of characteristic times obtained for a correlation output proportional to the concentration of the photoswitcher displays a maximum for the expected photoswitching characteristic time of Dronpa-2. The signal-to-noise ratio and the bandwidth of the spectrum agree with the theoretical predictions for the different weighting functions. The concentration of Dronpa-2 is deduced from the value of the correlation output at the extremum. In a second application, the titration of calcium is achieved using the reversibly photoswitchable sensor GCaMP6s-Q.[23, 20] A scaled correlation output independent of the concentration of the calcium sensor leads to spectra of characteristic times with different extrema for different calcium concentrations. The signal-to-noise ratio is in satisfying agreement with the theoretical predictions. Different titration curves of calcium are obtained using the scaled output associated with two well-chosen characteristic times close to the arguments of the extrema of the spectra.

The discrimination power and the signal-to-noise ratio of the correlation method are satisfactorily compared with the corresponding results of some other methods used in data processing of fluorescence photoswitching.

The Out-of-Phase Imaging after Optical Modulation (OPIOM and Speed-OPIOM) method involves a periodic illumination leading to periodic input fluorescence time series.[5, 6] OPIOM exploits an illumination at a single wavelength, whereas Speed-OPIOM harnesses two-wavelength illuminations in antiphase. The OPIOM or Speed-OPIOM output is the quadrature Fourier component of the time series given in Eq. (B.5) which shows a resonant behavior when the control parameters of illumination match the photoswitching kinetics. This quantity evaluated over one period compares well with the output deduced from the correlation method given in Eq. (2) for the weighting function h. Following the same lines as for the correlation method, we compute the signal-to-noise ratios and the ratio bandwidths for OPIOM and Speed-OPIOM. The results are given in section B.2. According to Eq. (B.7) and Tab. A.2 for the weighting function h, we find that OPIOM and the correlation method lead to close scaled signal-to-noise ratios 0.222 and 0.283, respectively. The comparison of the bandwidths is in favor of the correlation method since we find $W = 23$ for OPIOM and $W_{\beta^*} = 12$ for the correlation method. The scaled signal-to-noise ratio of Speed-OPIOM is equal to 0.443 and the associated ratio bandwidth is $W = 57$. If the optimization of the signal-to-noise ratio is the key point,

Speed-OPIOM is more competitive than the correlation method using h. However, Speed-OPIOM compares with the correlation method using a. If the discrimination power is more critical, Speed-OPIOM does not compete with the correlation method which is almost five times more selective. Nevertheless, the bandwidths of OPIOM and Speed-OPIOM are evaluated in a 2-D space of illumination parameters instead of the 1-D space of characteristic time for the correlation method. The comparison of the bandwidths in the different methods is therefore debatable.

The computation of correlations has already been harnessed in fluorescence imaging. The optical lock-in detection (OLID) method[12, 13] relies on the computation of correlation coefficients using an experimental weighting function without specification of the limit of integration and for a periodic illumination unrelated to the photoswitching kinetics. The q-OLID protocol[13] introduces the weighting function a for a fixed value of the characteristic time of the input time series still without recommendation on the limit of integration. The correlation method extends OLID to different weighting functions. It explores the possibility to exploit the computation of correlations in order to singularize the targeted characteristic time. In addition, the signal-to-noise ratio is optimized.

A spectrum of characteristic times contains more information than the collection of the extrema and the whole spectrum could be harnessed for discrimination purposes using methods developed for absorption or emission spectra, such as linear unmixing.[29, 30] The entire spectra obtained for several weighting functions could be processed using machine learning algorithms in order to optimize the selectivity and the sensitivity of discrimination. Eventually, the correlation method is not restricted to fluorescence input data and promises multiple applications in various fields of analytical chemistry.

Acknowledgements The authors thank Vincent Gielen and Peter Dedecker for providing the GCaMP6s-Q plasmid.

Funding This work was supported by the French national research agency [France BioImaging - ANR-10-INBS-04, Morphoscope2 - ANR-11-EQPX-0029, IPGG - ANR-10-IDEX-0001-02 PSL, ANR-10-LABX-31, ANR-19-CE11-0005, and ANR-19-CE29-0003-01], the Fondation de la Recherche Médicale [FRM DEI201512440], Sorbonne Université [Emergence 2019–2020, LIGHTNING], the Mission Interdisciplinarité of CNRS, the European Union Horizon 2020 research and innovation program MSCA-IF grant [SmartSAST 890479], and the EIC Pathfinder Open 2021 (DREAM). The funding sources had no involvement in study design; in the collection, analysis and interpretation of data; in the writing of the report; and in the decision to submit the article for publication.

A Tables of results deduced from the correlation method for a monoexponential input time series

Label	Weighting function $w_{\beta,\tau}(t)$
a	$\exp(-t/\tau) - (\exp(-\beta) - 1)/2$
b	1 for $0 \leq t^* < 0.1$, 0.309 for $0.1 \leq t^* < 0.25$, -0.196 for $0.25 \leq t^* < 1$
c	1 for $0 \leq t^* < 0.25$, $-1/3$ for $0.25 \leq t^* < 1$
d	1 for $0 \leq t^* < 0.5$, -1 for $0.5 \leq t^* < 1$
e	$\sin(2\pi t^*)$
f	$4t^*$ for $0 \leq t^* < 0.25$, $2 - 4t^*$ for $0.25 \leq t^* < 0.75$, $4t^* - 4$ for $0.75 \leq t^* < 1$
g	$1 - 4t^*$ for $0 \leq t^* < 0.5$, $4t^* - 3$ for $0.5 \leq t^* < 1$
h	$\cos(2\pi t^*)$
i	1 for $0 \leq t^* < 1/7$, $-3/4$ for $1/7 \leq t^* < 3/7$, $1/8$ for $3/7 \leq t^* < 1$
j	1 for $0 \leq t^* < 0.25$, -1 for $0.25 \leq t^* < 0.75$, 1 for $0.75 \leq t^* < 1$
k	1 for $0 \leq t^* < 1/3$, -2 for $1/3 \leq t^* < 2/3$, 1 for $2/3 \leq t^* < 1$
l	1 for $0 \leq t^* < 1/15$, $-7/8$ for $1/15 \leq t^* < 3/15$, $7/32$ for $3/15 \leq t^* < 7/15$, $-1/64$ for $7/15 \leq t^* < 1$
m	1 for $0 \leq t^* < 0.25$, -3 for $0.25 \leq t^* < 0.5$, 3 for $0.5 \leq t^* < 0.75$, -1 for $0.75 \leq t^* < 1$
n	1 for $0 \leq t^* < 1/5$, -4 for $1/5 \leq t^* < 2/5$, 6 for $2/5 \leq t^* < 3/5$, -4 for $3/5 \leq t^* < 4/5$, 1 for $4/5 \leq t^* < 1$
o	1 for $0 \leq t^* < 1/6$, -5 for $1/6 \leq t^* < 2/6$, 10 for $2/6 \leq t^* < 3/6$, -10 for $3/6 \leq t^* < 4/6$, 5 for $4/6 \leq t^* < 5/6$, -1 for $5/6 \leq t^* < 1$

Table A.1: Definition of the weighting functions $w_{\beta,\tau}(t)$ for $t^* = t/\beta\tau$, $0 \leq t^* \leq 1$

Weighting function	β^*	$M = O_{\beta^*}(\tau_m)/A$	W_{β^*}	$SNR^O_{\beta^*}(\tau_m)\epsilon\sqrt{n_0}/(A\sqrt{\tau_m})$
a	3.2453	0.0661399	25.7	0.463297
b	4.02922	0.0888158	27.146	0.471226
c	3.4634	0.12979	21.839	0.418365
d	2.51286	0.203632	18.3417	0.322798
e	2.35656	0.126308	15.1883	0.274212
f	2.33517	0.0988205	14.8699	0.261557
g	6.49061	0.0661399	12.64	0.291856
h	6.3532	0.079434	11.7641	0.283152
i	9.27263	0.0594356	11.7906	0.323761
j	6.09996	0.0955947	10.5587	0.236101
k	5.71144	0.107906	9.75529	0.182348
l	21.8204	0.0264042	10.0263	0.289400
m	9.34665	0.0712474	7.59153	0.097412
n	13.302	0.052322	6.59432	0.051001
o	17.5098	0.0409256	6.01209	0.026425

Table A.2: **Properties of the output $O_\beta(\tau)$ for the 15 weighting functions $a-o$ and the theoretical monoexponential input time series.** Optimal value of the limit of integration β^* such that the output $O_{\beta^*}(\tau_m)$ and the signal-to-noise ratio $SNR_{\beta^*}(\tau_m)$ are maximum, scaled output at the extremum $M = O_{\beta^*}(\tau_m)/A$, ratio bandwidth W_{β^*} of the output $O_{\beta^*}(\tau)$, scaled signal-to-noise ratio $SNR^O_{\beta^*}(\tau_m)\epsilon\sqrt{n_0}/(A\sqrt{\tau_m})$ at the maximum.

Weighting function	$\lvert\lim_{\tau\to 0}\Omega_\beta(\tau)\rvert$	β^*	$\lvert\Omega_{\beta^*}(\tau_m)\rvert$	$SNR^{\Omega}_{\beta^*}(\tau_m)\epsilon\sqrt{n_0}/(A\sqrt{\tau_m})$
a	$\frac{\sqrt{6}}{\beta}\sqrt{\frac{(\beta-2)\exp(\beta)+\beta+2}{\exp(\beta)-1}}$	$]0,\infty[$	1	$\propto \epsilon\sqrt{n_0}/A$
b	0.718207	6.7951	0.952524	1.85922
c	0.75	4.10158	0.877611	0.940792

Table A.3: **Properties of the scaled output $\Omega_\beta(\tau)$ for the weighting functions $a-c$ and the theoretical monoexponential input time series.** Limit of the scaled output $\Omega_\beta(\tau)$ when $\tau\to 0$, optimal value of the limit of integration β^* such that the scaled output $\Omega_{\beta^*}(\tau_m)$ is extremum, absolute extremum value $\lvert\Omega_{\beta^*}(\tau_m)\rvert$ of scaled output, scaled signal-to-noise ratio $SNR^{\Omega}_{\beta^*}(\tau_m)\epsilon\sqrt{n_0}/(A\sqrt{\tau_m})$ at the maximum.

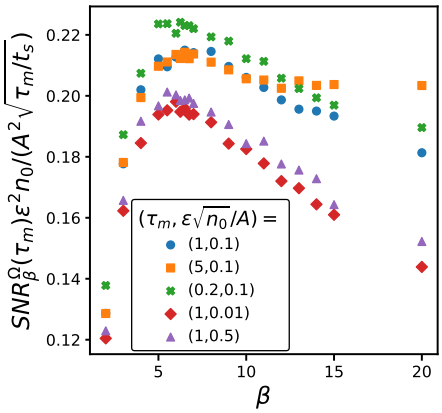

Figure A.1: Scaled signal-to-noise ratio $SNR^{\Omega}_{\beta}(\tau_m)\epsilon^2 n_0/(A^2\sqrt{\tau_m/t_s})$ of the scaled output associated with the weighting function a versus β with the sampling time $t_s = 0.01$.

Weighting function	$\beta^\dagger$	$M = \lvert\Omega_{\beta^\dagger}(\tau_m)\rvert$	$SNR^{\Omega}_{\beta^\dagger}(\tau_m)\epsilon\sqrt{n_0}/(A\sqrt{\tau_m})$	$\tau^\dagger/\tau_m$
a	6.5	1	$0.211\ \epsilon\sqrt{n_0}/A$	1
b	7.237	0.951999	1.87127	0.938939
c	5.271	0.870494	0.988255	0.778141

Table A.4: **Properties of the scaled output $\Omega_\beta(\tau)$ for the weighting functions $a-d$ and the theoretical monoexponential input time series.** Optimal value of the limit of integration $\beta^\dagger$ such that the signal-to-noise ratio $SNR^{\Omega}_{\beta^\dagger}(\tau_m)$ is maximum, absolute extremum value $\lvert\Omega_{\beta^\dagger}(\tau_m)\rvert$ of scaled output, scaled signal-to-noise ratio $SNR^{\Omega}_{\beta^\dagger}(\tau_m)\epsilon\sqrt{n_0}/(A\sqrt{\tau_m})$ at the maximum, scaled characteristic time $\tau^\dagger$ such that the scaled output $\Omega_{\beta^\dagger}(\tau^\dagger)$ is extremum.

Weighting function	$\lvert\lim_{\tau\to 0}\Omega_\beta(\tau)\rvert$	$\beta^\dagger$	$M = \lvert\Omega_{\beta^\dagger}(\tau_m)\rvert$	$SNR^{\Omega}_{\beta^\dagger}(\tau_m)\epsilon\sqrt{n_0}/(A\sqrt{\tau_m})$
d	0.866025	3.247	0.771779	0.562449
e	0.779697	3.193	0.667057	0.411438
f	0.75	3.222	0.635428	0.379881

Table A.5: **Properties of the scaled output $\Omega_\beta(\tau)$ for the weighting functions $d-f$ and the theoretical monoexponential input time series.** Limit of the scaled output $\Omega_\beta(\tau)$ when $\tau\to 0$, optimal value of the limit of integration $\beta^\dagger$ such that the signal-to-noise ratio $SNR^{\Omega}_{\beta^\dagger}(\tau_m)$ is maximum, absolute extremum value $\lvert\Omega_{\beta^\dagger}(\tau_m)\rvert$ of scaled output, scaled signal-to-noise ratio $SNR^{\Omega}_{\beta^\dagger}(\tau_m)\epsilon\sqrt{n_0}/(A\sqrt{\tau_m})$ at the maximum.

Weighting function	β^*	$\lvert\Omega_{\beta^*}(\tau_m)\rvert$	W_{β^*}	$SNR^{\Omega}_{\beta^*}(\tau_m)\epsilon\sqrt{n_0}/(A\sqrt{\tau_m})$
g	9.73738	0.524337	35.5395	0.388138
h	9.18002	0.508215	28.2981	0.369035
i	14.331	0.559041	22.1169	0.442243
j	8.34391	0.424012	22.018	0.288687
k	7.42446	0.329731	19.8781	0.211142
l	34.173	0.473301	18.4173	0.368636
m	12.285	0.163102	13.9305	0.106962
n	17.25	0.0823689	12.2859	0.0549499
o	22.396	0.0417837	11.4372	0.0282201

Table A.6: **Properties of the scaled output $\Omega_\beta(\tau)$ for the weighting functions $g-o$ and the theoretical monoexponential input time series.** Optimal value of the limit of integration β^* such that the output $\Omega_{\beta^*}(\tau_m)$ is extremum, absolute extremum value $\lvert\Omega_{\beta^*}(\tau_m)\rvert$ of scaled output, ratio bandwidth W_{β^*} of the scaled output $\Omega_{\beta^*}(\tau)$, scaled signal-to-noise ratio $SNR^{\Omega}_{\beta^*}(\tau_m)\epsilon\sqrt{n_0}/(A\sqrt{\tau_m})$ at the maximum.

Weighting function	$\beta^\dagger$	$M=\lvert\Omega_{\beta^\dagger}(\tau_m)\rvert$	$W_{\beta^\dagger}$	$SNR^{\Omega}_{\beta^\dagger}(\tau_m)\epsilon\sqrt{n_0}/(A\sqrt{\tau_m})$	$\tau^\dagger/\tau_m$
g	11.149	0.521463	36.2003	0.391462	0.873386
h	10.466	0.505249	28.8314	0.372344	0.877128
i	15.316	0.558075	22.2325	0.443428	0.935688
j	9.552	0.420872	22.5282	0.291717	0.873525
k	8.622	0.326396	20.505	0.213996	0.861107
l	35.102	0.473151	18.4335	0.368791	0.973526
m	13.234	0.16257	14.0533	0.107341	0.928326
n	18.069	0.0822496	12.3319	0.0550326	0.954669
o	23.134	0.0417514	11.4595	0.0282423	0.968113

Table A.7: **Properties of the scaled output $\Omega_\beta(\tau)$ for the weighting functions $g-o$ and the theoretical monoexponential input time series.** Optimal value of the limit of integration $\beta^\dagger$ such that the signal-to-noise ratio $SNR^{\Omega}_{\beta^\dagger}(\tau_m)$ is maximum, absolute extremum value $\lvert\Omega_{\beta^\dagger}(\tau_m)\rvert$ of scaled output, ratio bandwidth $W_{\beta^\dagger}$ of the scaled output $\Omega_{\beta^\dagger}(\tau)$, scaled signal-to-noise ratio $SNR^{\Omega}_{\beta^\dagger}(\tau_m)\epsilon\sqrt{n_0}/(A\sqrt{\tau_m})$ at the maximum, scaled characteristic time $\tau^\dagger$ such that the scaled output $\Omega_{\beta^\dagger}(\tau^\dagger)$ is extremum.

B Signal-to-noise ratios and bandwidths for other methods of fluorescence data processing

B.1 $\Delta I/I(0)$

The relative fluorescence variation during constant illumination

$$\frac{\Delta I}{I(0)} = \frac{I(0) - I(\infty)}{I(0)} \tag{B.1}$$

gives information on the kinetics of reversibly photoswitchable fluorophore [23, 20].

When the input time series $I(t)$ is a monoexponential function of prefactor A and baseline

offset B, Eq. (B.1) becomes

$$\frac{\Delta I}{I(0)} = \frac{A}{A+B} \tag{B.2}$$

We use Eqs. (3-7) in which $I(t)$ has been replaced by $\frac{\Delta I}{I(0)}$ and we perform an expansion in $\epsilon \ll 1$ to compute the output noise

$$N^{\frac{\Delta I}{I(0)}} = \frac{\epsilon}{A+B}\sqrt{n_0\left(\left(\frac{A}{A+B}\right)^2 - 4\frac{A}{A+B} + 4\right)} \tag{B.3}$$

The signal-to-noise ratio is

$$SNR^{\frac{\Delta I}{I(0)}} = \frac{A}{\epsilon\sqrt{n_0\left(\left(\frac{A}{A+B}\right)^2 - 4\frac{A}{A+B} + 4\right)}} \tag{B.4}$$

The relative fluorescence variation is independent of the characteristic time of the input time series. The kinetic information is included in the ratio A/B and $\frac{\Delta I}{I(0)}$ sensitively varies only for $|A/B| \sim 1$ as shown in Fig. B.1a. The relative fluorescence variation $\frac{\Delta I}{I(0)}$ behaves as a low-pass filter with respect to A/B and cannot be used for discrimination purposes between several photoswitching fluorophores.

Figure B.1b displays the variation of $\frac{\Delta I}{I(0)}$ versus calcium concentration, leading to a monotonous increase and an exploitable titration curve. The Hill function $a/(1+(K/[Ca^{2+}])^\nu + b$ is fitted to the titration curve. We obtain the characteristic concentration $K = 66.8$ nM and the Hill parameter $\nu = 3.32$. These values are similar the results obtained using the correlation method.

The relative fluorescence variation $\frac{\Delta I}{I(0)}$ are calculated for each of the 3072 time series $I(t)$. Equations (6, 7) are used to estimate the mean $\langle\frac{\Delta I}{I(0)}\rangle = 0.6076$ and the signal-to-noise ratio. The signal-to-noise ratios $SNR^{\frac{\Delta I}{I(0)}}\epsilon\sqrt{n_0}/A\sqrt{\tau_m^B})$ predicted for a monoexponential input time series are given in Eq. (B.4). The factor $A/\epsilon\sqrt{n_0} = 11.2$ and $\frac{A}{A+B} = 0.6076$ are used to compare the predictions with the experimental results. The experimental normalized histograms and the probability density functions of the normal laws of mean value $\langle\Delta I/I(0)\rangle$ and standard deviations $\langle\Delta I/I(0)\rangle SNR^{\frac{\Delta I}{I(0)}}$ are shown in Fig. 4d. The experimental standard deviation is smaller than the theoretical prediction due to the failure of the monoexponential hypothesis about the input time series.

B.2 Out-of-Phase Imaging after Optical Modulation (OPIOM and Speed OPIOM)

The reversible photoswitching of a fluorescent species may be induced by illumination at a single wavelength or two wavelengths.[5, 6] A sinewave illumination of period T and mean intensity I_1^0 at one wavelength is used in the Out-of-Phase Imaging after Optical Modulation (OPIOM) protocol whereas two sine waves of period T in antiphase and mean intensities I_1^0 and I_2^0 at

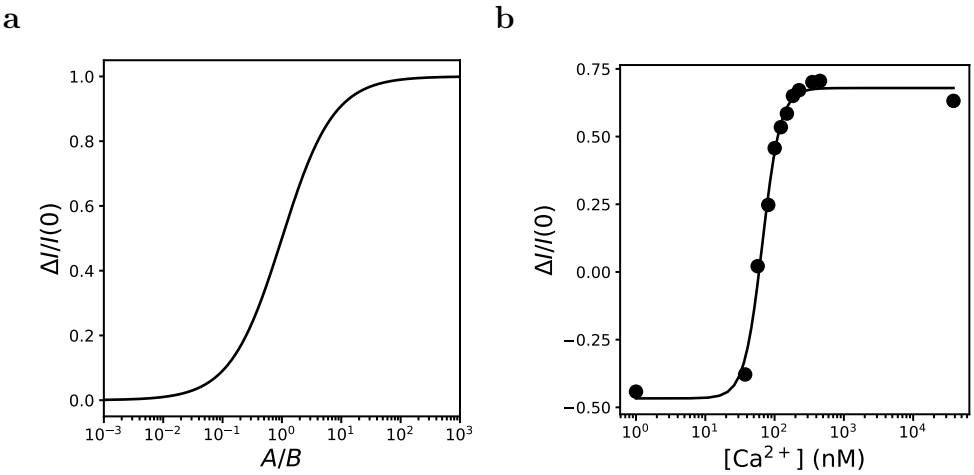

Figure B.1: **a**: Relative fluorescence variation $\Delta I/I(0)$ versus A/B. **b**: Titration curve $\Delta I/I(0)$ versus [Ca^{2+}]. The line give the fitted Hill functions to the experimental results (symbols).

two wavelengths are used in Speed-OPIOM. For both methods, the resulting fluorescence time series $I(t)$ are T-periodic and the quadrature Fourier coefficients $Q(\omega, I_1^0, I_2^0)$ are computed in the same way with $I_2^0 = 0$ for OPIOM. We obtain

$$Q(\omega, I_1^0, I_2^0) = \frac{2}{kT} \int_0^{kT} I(t) \cos(\omega t)\, \mathrm{d}t \tag{B.5}$$

where $\omega = 2\pi/T$ is the angular frequency and k is the number of analyzed periods of the input time series $I(t)$. We use Eqs. (2-6) in which $I(t)$ has been replaced by $Q(\omega, I_1^0, I_2^0)$ to compute the output noise N^Q associated with the quadrature Fourier coefficient

$$N^Q = \frac{2\epsilon}{kT} \sqrt{n_0 \int_0^{kT} \cos(\omega t)^2\, \mathrm{d}t} \tag{B.6}$$

The case of a two-state photoswitching reaction scheme of characteristic time τ_m is considered. The experimental parameters, i.e. the mean light intensities I_1^0 and I_2^0 and the angular frequency ω, are chosen in order to optimize the quadrature Fourier coefficient. In particular the period is set at $T = 2\pi\tau_m$.[5, 6] The optimum value of $Q(\omega, I_1^0, I_2^0)$ is equal to $0.125A$ for an illumination at one wavelength and $0.25A$ for a two-wavelength illumination, where A is the mean fluorescence amplitude.[5, 6] Consequently the signal-to-noise ratio is

$$SNR^Q = \frac{0.222A\sqrt{k\tau_m}}{\epsilon\sqrt{n_0}} \tag{B.7}$$

for OPIOM and

$$SNR^Q = \frac{0.443A\sqrt{k\tau_m}}{\epsilon\sqrt{n_0}} \tag{B.8}$$

The ratio bandwiths of the quadrature Fourier coefficients in the 2-D space (I_1^0, ω) for OPIOM and $(I_2^0/I_1^0, \omega/I_1^0)$ for Speed-OPIOM are equal to $W = 23.482$ and $W = 57.442$, respectively.[5, 6]

References

[1] J. R. Lakowicz, H. Szmacinski, K. Nowaczyk, K. W. Berndt, and M. L. Johnson. Fluorescence lifetime imaging. *Anal. Biochem.*, 202:316–330, 1992.

[2] P. I. Bastiaens and A. Squire. Fluorescence lifetime imaging microscopy: spatial resolution of biochemical processes in the cell. *Trends Cell Biol.*, 9:48–52, 1999.

[3] T. Sandén, G. Persson, P. Thyberg, H. Blom, and J. Widengren. Monitoring kinetics of highly environment sensitive states of fluorescent molecules by modulated excitation and time-averaged fluorescence intensity recording. *Anal. Chem.*, 79(9):3330–3341, 2007.

[4] C. I. Richards, J.-C. Hsiang, and R. M. Dickson. Synchronously amplified fluorescence image recovery (SAFIRe). *J. Phys. Chem. B*, 114:660–665, 2010.

[5] J. Quérard, T.-Z. Markus, M.-A. Plamont, C. Gauron, P. Wang, A. Espagne, M. Volovitch, S. Vriz, V. Croquette, A. Gautier, T. Le Saux, and L. Jullien. Photoswitching kinetics and phase-sensitive detection add discriminative dimensions for selective fluorescence imaging. *Angew. Chem. Int. Ed.*, 127:2671–2675, 2015.

[6] J. Quérard, R. Zhang, Z. Kelemen, M.-A. Plamont, X. Xie, R. Chouket, I. Roemgens, Y. Korepina, S. Albright, E. Ipendey, M. Volovitch, H. L. Sladitschek, P. Neveu, L. Gissot, A. Gautier, J.-D. Faure, V. Croquette, T. Le Saux, and L. Jullien. Resonant out-of-phase fluorescence microscopy and remote imaging overcome spectral limitations. *Nat. Comm.*, 8:969, 2017.

[7] R. Zhang, R. Chouket, M.-A. Plamont, Z. Kelemen, A. Espagne, A. G. Tebo, A. Gautier, L. Gissot, J.-D. Faure, L. Jullien, V. Croquette, and T. Le Saux. Macroscale fluorescence imaging against autofluorescence under ambient light. *Light Sci. Appl.*, 7:97, 2018.

[8] R. Zhang, R. Chouket, A. G. Tebo, M.-A. Plamont, Z. Kelemen, L. Gissot, J.-D. Faure, A. Gautier, V. Croquette, L. Jullien, and T. Le Saux. Simple imaging protocol for autofluorescence elimination and optical sectioning in fluorescence endomicroscopy. *Optica*, 6(8):972–980, 2019.

[9] A. Orth, R. N. Ghosh, E. R. Wilson, T. Doughney, H. Brown, P. Reineck, J. G. Thompson, and B. C. Gibson. Super-multiplexed fluorescence microscopy via photostability contrast. *Biomed. Opt. Express*, 9(7):2943–2954, 2018.

[10] H. Valenta, S. Hugelier, S. Duwé, G. L. Gerfo, M. Müller, P. Dedecker, and W. Vandenberg. Separation of spectrally overlapping fluorophores using intra-exposure excitation modulation. *Biophysical Reports*, 1(2):100026, 2021.

[11] R. Chouket, A. Pellissier-Tanon, A. Lahlou, R. Zhang, D. Kim, M.-A. Plamont, M. Zhang, X. Zhang, P. Xu, N. Desprat, D. Bourgeois, A. Espagne, A. Lemarchand, T. Le Saux, and L. Jullien. Extra kinetic dimensions for label discrimination. *Nat. Commun.*, 13:1482, 2022.

[12] G. Marriott, S. Mao, T. Sakata, J. Ran, D. K. Jackson, C. Petchprayoon, T. J. Gomez, E. Warp, O. Tulyathan, H. L. Aaron, E. Y. Isacoff, and Y. Yan. Optical lock-in detection imaging microscopy for contrast-enhanced imaging in living cells. *Proc. Natl. Acad. Sci. U. S. A.*, 105:17789–17794, 2008.

[13] G. Abbandonato, B. Storti, G. Signore, F. Beltram, and R. Bizzarri. Quantitative optical lock-in detection for quantitative imaging of switchable and non-switchable components. *Microsc. Res. Tech.*, 79(10):929–937, OCT 2016.

[14] T. Vettenburg, A. Corral, A. Rodríguez-Pulido, C. Flors, and J. Ripoll. Photoswitching-enabled contrast enhancement in light sheet fluorescence microscopy. *ACS Photonics*, 4(3):424–428, 2017.

[15] C. R. Crowell and S. Alipanahi. Transient distortion and nth order filtering in deep level transient spectroscopy (dnlts). *Solid State Electron.*, 24(1):25–36, 1981.

[16] A. A. Istratov. New correlation procedure for the improvement of resolution of deep level transient spectroscopy of semiconductors. *J. Appl. Phys.*, 82(6):2965–2968, 1997.

[17] A. A. Istratov. The resolution limit of traditional correlation functions for deep level transient spectroscopy. *Rev. Sci. Instrum.*, 68(10):3861–3865, 1997.

[18] A. A. Istratov, O. F. Vyvenko, H. Hieslmair, and E. R. Weber. Critical analysis of weighting functions for the deep level transient spectroscopy of semiconductors. *Meas Sci Technol*, 9(3):477, 1998.

[19] A. A. Istratov and O. F. Vyvenko. Exponential analysis in physical phenomena. *Rev. Sci. Instrum.*, 70(2):1233–1257, 1999.

[20] B. Adelizzi, V. Gielen, T. Le Saux, P. Dedecker, and L. Jullien. Quantitative model for reversibly photoswitchable sensors. *ACS sens.*, 6(3):1157–1165, 2021.

[21] Franziska Bierbuesse, Anaïs C Bourges, Vincent Gielen, Viola Mönkemöller, Wim Vandenberg, Yi Shen, Johan Hofkens, Pieter Vanden Berghe, Robert E Campbell, Benjamien Moeyaert, et al. Absolute measurement of cellular activities using photochromic single-fluorophore biosensors and intermittent quantification. *Nature Communications*, 13(1):1–13, 2022.

[22] R. Ando, C. Flors, H. Mizuno, J. Hofkens, and A. Miyawaki. Highlighted generation of fluorescence signals using simultaneous two-color irradiation on Dronpa mutants. *Biophys. J.*, 92:L97 – L99, 2007.

[23] V. Gielen, V. Mönkemöller, Y. Shen, J. Hofkens, P. Vanden Berghe, R. E. Campbell, B. Moeyaert, and P. Dedecker. Absolute measurement of cellular activities using photochromic single-fluorophore biosensors. *bioRxiv*, 2020.

[24] J. Schoukens and J. Renneboog. Modeling the noise influence on the fourier coefficients after a discrete fourier transform. *IEEE Trans. Instrum. Meas.*, IM-35(3):278–286, 1986.

[25] K. Dmowski and Z. Pioro. Theoretical signal-to-noise ratio for correlators with linear averaging. *Rev. Sci. Instrum.*, 58(1):75–77, 1987.

[26] D. Summers and J. M. W. Scott. Systems of first-order chemical reactions. *Mathematical and Computer Modelling*, 10(12):901–909, 1988.

[27] D. T. Gillespie. The chemical Langevin equation. *J. Chem. Phys.*, 113(1):297–306, 2000.

[28] R. Ando, H. Mizuno, and A. Miyawaki. Regulated fast nucleocytoplasmic shuttling observed by reversible protein highlighting. *Science*, 306:1370–1373, 2004.

[29] T. Zimmermann. Spectral imaging and linear unmixing in light microscopy. In *Microscopy techniques*, volume 95, pages 245–265. Springer, Berlin, heidelberg edition, 2005.

[30] T. Zimmermann, J. Marrison, K. Hogg, and P. O'Toole. Clearing up the signal: spectral imaging and linear unmixing in fluorescence microscopy. In *Confocal microscopy*, volume 1075, pages 129–148. Springer, New York, NY, 2014.